MASS FLOWMETER USING A MULTI-SENSOR CHIP

Yong Xu, Chen-Wei Chiu*, Fukang Jiang, Qiao Lin and Yu-Chong Tai

Electrical Engineering, California Institute of Technology, Pasadena, CA 91125, USA
*Umachines Inc., 3360 E. Foothill, Pasadena, CA 91107, USA

ABSTRACT

We report here a novel two-mode mass flowmeter that can be operated in either thermal or differential pressure mode. By combining these two complementary operating principles, the performance can be improved significantly. This flowmeter is based on a multi-sensor chip that includes a 1-D array of shear stress, pressure and temperature sensors. The multi-sensor chip can also be employed in many other complicated channel flow studies. Extensive tests have been carried out on shear stress sensors to evaluate the effects of overheat ratio, channel height and gas properties.

INTRODUCTION

Silicon thermal flowmeters can be dated back to 1974 [1], and [2,3] provide excellent reviews. Thermal anemometry is one of the most widely used principles. The advantage of thermal flowmeter is its high sensitivity. One factor that limits the sensitivity is the heat loss from the heating element to the substrate. To reduce the heat loss, many structures such as closed membranes, cantilever beams, bridges and suspended membranes have been proposed and fabricated [2]. In our lab, a thermal shear stress sensor, which is a polysilicon resistor sitting on a nitride diaphragm with a vacuum cavity underneath, has been successfully developed [4-6]. Heat loss to substrate is greatly reduced and a higher sensitivity is achieved. A very sensitive thermal flowmeter can be fabricated based on this vacuum cavity scheme. But the disadvantages are its non-linear output and long term drift due to the elevated operating temperature.

The differential pressure principle is another well-known approach for mass flow rate measurements. It is less sensitive to ambient temperature and has a linear relationship between the pressure drop and flow rate in the laminar flow regime. However, to obtain a high sensitivity, a significant pressure drop should be created which is not acceptable in many applications.

Thermal and differential pressure approaches have their respective advantages and disadvantages. As a matter of fact, their performances are complementary. We successfully developed a novel flowmeter combining both thermal and differential pressure principles. This flowmeter is based on a multi-sensor chip that includes a 1-D array of shear stress and pressure sensors, as well as temperature sensors for temperature compensation.

DESIGN, FABRICATION AND PACKAGING

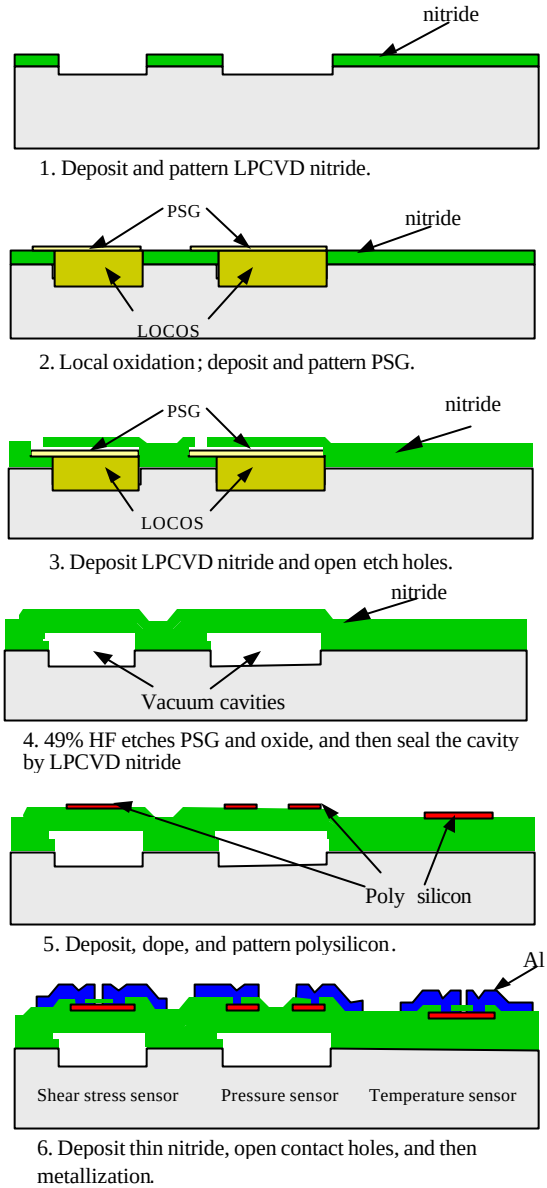

Figure 1 Simplified fabrication process.

The multi-sensor chip contains five sensor clusters, with a pitch of 2 mm, consisting of shear stress, pressure and temperature sensors. The structure of the shear stress sensor is the same as that in [5,6], and the fabricatoion

process is shown in Fig. 1. The sensing element, i.e. the thin film polysilicon resistor, is embedded in a 210x210 μm^2 silicon nitride diaphragm with a vacuum cavity underneath to minimize the heat loss to the silicon substrate. The resistor is 7 μm wide and 150 μm long with a typical resistance of 1.4 kΩ at the room temperature. The pressure sensor employs the piezoresistive effect of polysilicon. Polysilicon piezoresistors are deposited on a vacuum-sealed nitride diaphragm and provide an electrical output that is proportional to the deflection of the diaphragm [7]. To increase the sensitivity of the pressure sensor, we implemented a bossed diaphragm design. The temperature sensor is a circular polysilicon thermistor with a typical resistance of 4 kΩ. The process starts with the deposition and patterning of low stress silicon nitride on silicon wafers. Windows are etched further into silicon to form a 1-μm-deep trench. 2 μm of thermal oxide is grown on the trench, and then the wafers are planarized by HF dip. A 400-nm-thick PSG (phosphosilicate glass) layer is deposited, patterned and annealed to form the etching channels. Next, about 1.5 μm low-stress nitride is deposited and patterned, opening the etching holes. PSG and thermal oxide are etched away by 49% HF and the nitride diaphragms are released. After this,

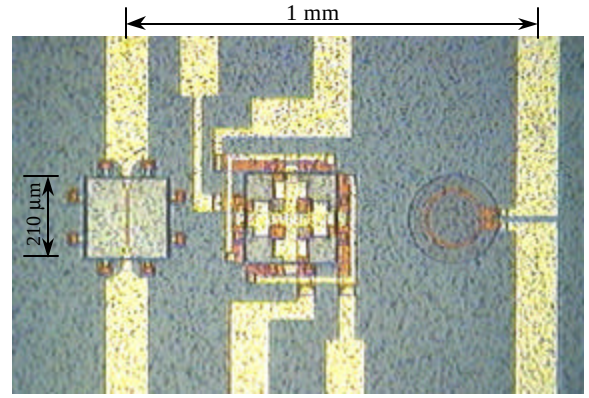

(a)

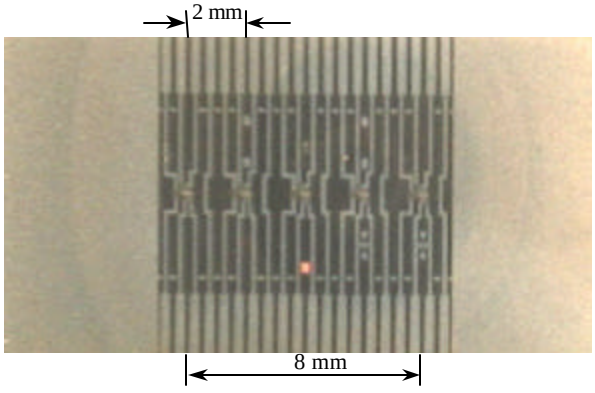

(b)

Figure 2 (a) Picture of one sensor cluster.
(b) Picture of a multi-sensor array chip.

the cavities are sealed by a deposition of another layer of nitride, and the diaphragms of the pressure sensors are patterned to form the beam and bossed structures. A 500-nm-thick polysilicon film is then deposited, doped and patterned to form the sensing resistors. The polysilicon films are doped twice. The first doping is a global boron ion implantation with a dose of $1\times10^{15}/cm^2$ to obtain a nearly zero temperature coefficient of resistance (TCR). The second doping is a selective high-dose boron ion implantation ($1\times10^{16}/cm^2$) on the shear stress, temperature sensors and also on the contacts and turning sections of the pressure resistors to minimize the connection resistance. Another 180-nm-thick nitride is deposited as a passivation layer and is followed by contact hole opening and aluminum metallization. Finally the multi-sensor chip is diced into 2×1 cm^2 chips and Fig. 2 shows one sensor cluster and a complete multi-sensor chip.

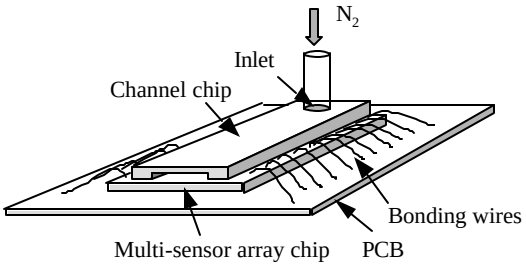

(a)

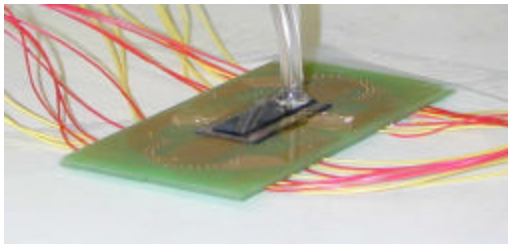

(b)

Figure 3 (a) Schematic of packaged device.
(b) Real picture of packaged device.

To assemble the mass flowmeter, the multi-sensor chip is first bonded to a printed circuit board and then another channel chip (the channel is 2.5-mm wide and 18-mm long) is flip-bonded on top of the sensor chip as shown in Fig. 3. To determine the effect of channel height, three different channels with heights of 150 μm, 200 μm and 288 μm are fabricated by DRIE. The first sensor cluster is 4 mm away from the inlet to ensure all the sensors are in fully developed flow. The pressure and temperature sensors are then calibrated before various flow measurements. Due to the bossed-diaphragm design, the sensitivity of the pressure sensor is 570 μV/(psi•V) which is much higher than those using uniform diaphragms [7].

OPERATING PRINCIPLES

The temperature sensor is a polysilicon thermistor and the operation is very straightforward. The principle of pressure sensor has been mentioned briefly in the fabrication section. More detailed information can be found in [7]. Here we only focus on the shear stress sensor, which is a heated resistor sitting on a vacuum cavity. The input power of the resistor is a function of the wall shear stress of the ambient fluid, which is defined by

$$t = m \left. \frac{dU}{dy} \right|_{y=0} \tag{1}$$

where m is the fluid's viscosity, U is the streamwise velocity and y is normal to and originates at the sensor surface. The relationship between τ and the input power P to the sensor is typically described by [8]:

$$P = \frac{V^2}{R_S} = \Delta T(A(rt)^{1/3} + B) \tag{2}$$

where V and R_S are respectively the voltage and resistance of shear stress sensor, DT is the temperature difference between the heated resistor and ambient, $A \propto C_p^{1/3} k_T^{2/3} / m^{1/3}$ (C_p and k_T are the heat capacity and thermal conductivity of the fluid respectively), r is the density of the fluid and term B represents the heat loss to the substrate. However, Eq.2 is derived for conventional macro heating element and may not be valid for our micromachined shear stress sensor. In this case, we use the empirical formula

$$P = \frac{V^2}{R_S} = \Delta T(A_t(rt)^{1/n} + B_t) \tag{3}$$

where A_t, B_t and n are determined experimentally.

For the rectangular channel flow, if the height h is much smaller than the width (which is true in our case), the relationship between τ and the pressure gradient dp/dx along the channel is [9]

$$t = \frac{h}{2}\frac{dp}{dx}. \tag{4}$$

On the other hand, in the laminar flow regime the flow rate Q is given by [9]

$$Q = \frac{h^3 w}{12m}\frac{dp}{dx} \quad . \tag{5}$$

Note that Eq.5 is also the principle for differential pressure based flow rate measurement. Combining Eqs. 3,4 and 5, we obtain the relationship between the input power and the flow rate in laminar flow regime

$$P = \frac{V^2}{R_S} = A_0 Q^{1/n} + B_0 \tag{6}$$

where $A_0 = \Delta T A_t (\frac{6rm}{h^2 w})^{1/n}$ and $B_0 = \Delta T B_t$.

The shear stress sensor operates in constant temperature (CT) mode, namely the temperature of the sensor remains constant during operation. Fig.4 shows the simplified CT biasing circuits, where R_S is the shear stress sensor, R_1 is adjustable and R_2 equals R_3. In addition, R_1, R_2 and R_3 have nearly zero TCR. R_S, R_1, R_2 and R_3, together with the operational amplifier, form a negative feedback loop which requires that R_S must equal R_1 when steady state is reached. An important parameter for the operation of shear stress sensor is the (resistive) overheat ratio, which is defined as

$$a_R = (R_S - R_{S0}) / R_{S0} \tag{7}$$

where R_S is the resistance of the shear stress sensor at the operating temperature and R_{S0} is the resistance at a reference temperature. For example, if an overheat ratio of 10% is desired, we then set R_1 = (1+10%) R_{S0}. Under normal operating condition, the Wheatstone bridge is balanced. Thus $R_1 = R_S$ and $V_{out} = 2V$. By measuring V_{out}, we know how much power is dissipated through fluid and hence the flow rate.

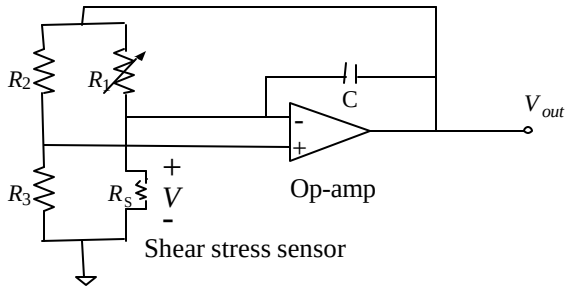

Figure 4 Simplified constant temperature bias circuit.

TESTING AND DISCUSSION

After calibration of pressure and temperature sensors, we first measure the temperature and pressure coefficients of the shear stress sensors. The pressure coefficient is between 1.9 mV/psi and 1.5 mV/psi. The temperature coefficient is about -50mV/°C, which is much larger than the pressure coefficient. Then we

obtain the pressure and temperature distributions as well as the relative output change of the shear stress sensors ($\Delta V/V_0$) in a fully developed incompressible flow (Q = 1.77 SLPM with a Mach number of 0.2). V_0 is the output voltage when the flow rate is zero and ΔV is the output voltage change at a non-zero flow rate. In Eq. (6), $V = V_0 + \Delta V$ and $B_0 = V_0^2 / R_S$. The term $(\Delta V/V_0)^2$ is negligible since $\Delta V/V_0 << 1$. Finally, we have

$$\frac{\Delta V}{V_0} \propto \frac{A_0}{2B_0} t^{1/n} \qquad (8)$$

Fig.5 shows that the pressure gradient and the temperature are almost constant. Base on channel flow theory [9], shear stress should also be constant along the channel. Because of process variation, there is non-uniformity among the five shear stress sensors even though they are on the same chip. If we use V or V^2 as the output, there are large variations from sensor to sensor. But as shown in Fig. 5 (c), if DV/V_0 is used, a much better sensor to sensor uniformity is obtained.

Fig. 6 then shows the case of compressible flow (Q = 9.46 SLPM with a Mach number of 0.6). We observe of nonlinear pressure drop, non-constant temperature distribution and shear stress variation along the channel. Note that in Fig 6 (c), the term $(\Delta V/V_0)^2$ is not negligible since it is relatively large in this case. Figs. 5 and 6 illustrate that pressure, temperature and shear stress distributions in both compressible and incompressible flows can be obtained simultaneously by using this multi-sensor chip. Therefore, in addition to the mass flowmeter, this multi-sensor chip can be employed in many other applications. For instance, in the case of micro nozzle flow, we need all three types of sensors to fully understand the highly complicated flow characteristics.

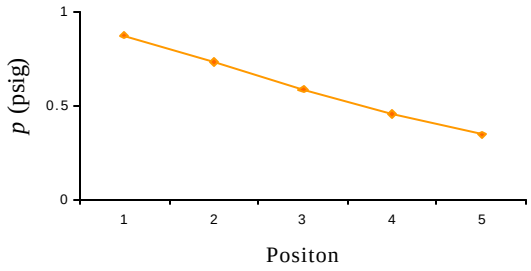

(a) Pressure distribution

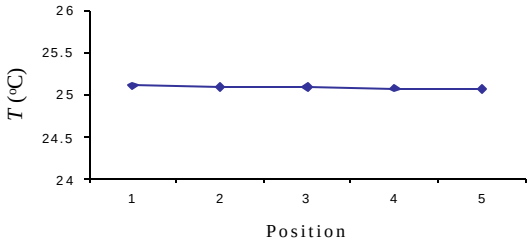

(b) Temperature distribution

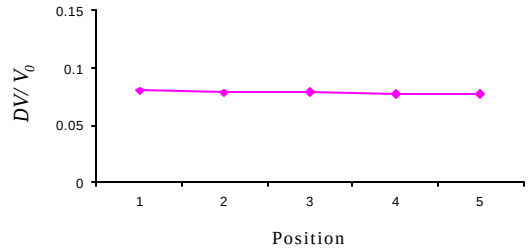

(c) Relative output change of shear stress sensors

Figure 5 Measurement of fully developed incompressible channel flow.

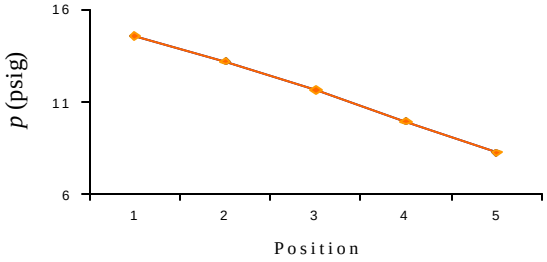

(a) Pressure distribution

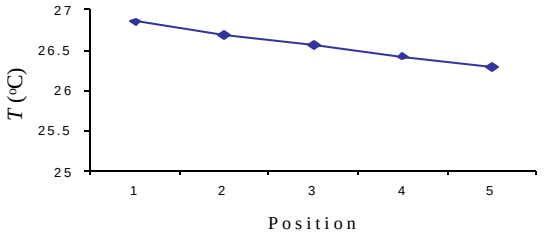

(b) Temperature distribution

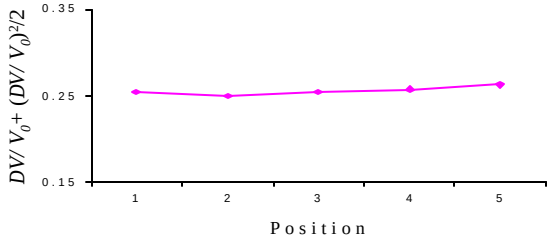

(c) Relative output change of shear stress sensor

Figure 6 Measurement of fully developed compressible channel flow.

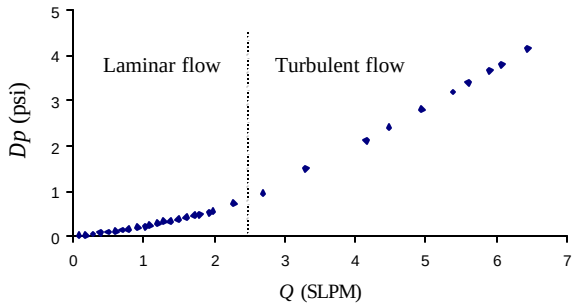

Figure 7 Pressure drop vs. mass flow rate (h=200 μm and N_2 flow).

Fig. 7 shows the pressure difference Δp of pressure sensors #1 and #5 varying with mass flow rate Q (in the channel with h = 200 μm and N_2 flow) in both laminar and turbulent flow regimes. The transition region for laminar and turbulent flow is around Q = 2.5 SLPM, where Re = 2100. The laminar flow data agree with what Eq.5 predicts. From laminar to turbulent flow, the slope of the curve increases. Therefore, in the turbulent flow regime, the pressure sensor based flowmeter is more sensitive even though there is no simple equation for the flow rate.

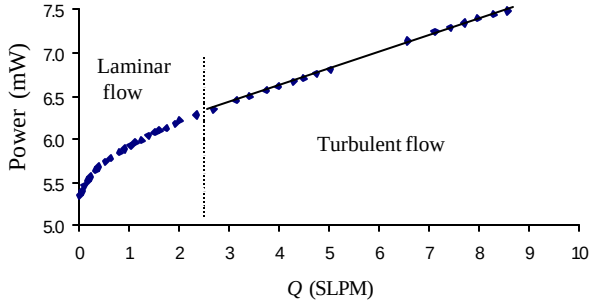

Figure 8 Response of shear stress sensor (h=200 μm, a_R = 10% and N_2 flow).

Fig. 8 shows the input power of shear stress sensor measured with a_R =10% and in a 200 μm high channel and nitrogen flow. One of the most severe problems of the hot film shear stress sensors is that the output is very sensitive to ambient temperature. Using the on-chip thermistor, the experimental data have been temperature compensated. Interestingly, we find that in the turbulent flow regime, the response of the shear stress sensor is almost linear. The advantage of CT mode is that sensor output will not saturate even for a very large mass flow rate thus the measurement range could be very wide. One thing we should pay attention to is that our thermal shear stress sensor has very short response time (with a system bandwidth of 10 kHz), which is an advantage in laminar flow measurement, but in turbulent flow, the sensor output will always fluctuate because of flow turbulence. Therefore, time averaging is necessary for turbulent flow measurement. Note that in the large flow rate case, the flow becomes both turbulent and compressible and the situation becomes very complicated.

According to Eq.6, dissipation power should be a linear function of $Q^{1/n}$ in laminar flow. Using the least squares method to fit the data, we obtain n = 2.2 which differs considerably from the conventional value of 3. Our group has long been working on MEMS thermal shear stress sensors [4-6]. For one time, the classical law of $P \propto \tau^{1/3}$ has been used to characterize our sensors. However, experimental data clearly show that the classical $P \propto \tau^{1/3}$ law is not valid in this case. In order to explain this, the first microscale heat transfer model for MEMS shear-stress sensors based on a systematic experimental and theoretical investigation is proposed by Lin *et al* [10]. Important microscale heat transfer effects ignored by classical theory are identified. Fig. 9 focuses on the laminar flow part of Fig. 8 by changing the horizontal axis to $Q^{1/2.2}$.

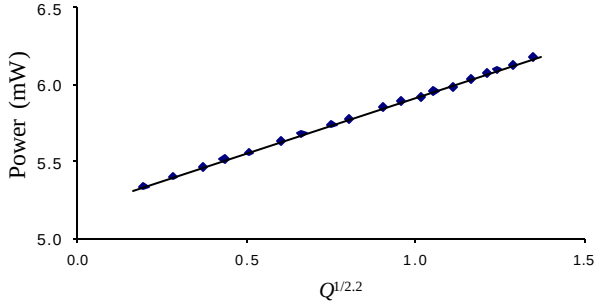

Figure 9 Input power versus $Q^{1/2.2}$ (laminar flow region).

With the vacuum cavity underneath, the heat loss to substrate is reduced significantly so that a very high sensitivity is obtained. It can be seen from Figure 10 that the sensitivity of the shear stress sensor is not constant. For example, at Q =1 SLPM, the sensitivity is 0.17 V/SLPM but at Q = 0.1 SLPM, it increases to 0.62 V/SLPM. This mass flowmeter has extremely high sensitivity at small flow rates, which is desirable for some applications.

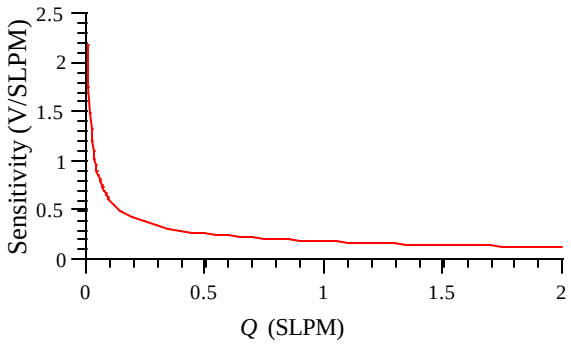

Figure 10 Sensitivity of the thermal flowmeter in laminar flow regime

As we can see, the advantage of thermal flowmeter is its high sensitivity. However, the output is not a linear function of flow rate and the biggest problem is the long term drift due to its elevated operating temperature. While in the laminar flow regime, the differential pressure based flowmeter has sensitivity only in the order of mV/SLPM, it is less sensitive to ambient temperature and has a simple linear relationship between the pressure drop and flow rate as shown in Eq.5. As a matter of fact, the performances of thermal and differential pressure based flowmeters are complementary. By combining these two principles into a single flowmeter, the performance can be significantly improved.

In order to fully understand the characteristics of the shear stress sensor based flowmeter, extensive tests have been carried out with different overheat ratios, channel heights and gases.

Table 1 compares experimental values of A_0 and B_0 for different overheat ratios both in nitrogen and helium flows in the 200 μm high channel. In order to compare A_0 and B_0, we need to fix n first. n should not change significantly with overheat ratio or gas, we use the averaged n which is 2.20.

Table 1 Experimental A_0 and B_0 for different a_R (h = 200 μm and n = 2.20)

Gas	over heat ratio	A_0	B_0
Nitrogen	5%	0.349	2.84
	10%	0.719	5.20
	20%	1.31	9.52
Helium	5%	0.706	3.64
	10%	1.31	6.87
	20%	2.30	13.0

From the above table, we can clearly see that when the overheat ratio doubles, A_0 and B_0 approximately double correspondingly. This can be explained by the following analysis. We know that the resistance of sensing element at temperature T is

$$R_S = R_{S0}[1 + \alpha_T (T - T_0)] \tag{9}$$

where R_{S0} is the resistance at reference temperature T_0 and α_T is the TCR of sensing element. Combined with Eq.7, we have

$$\alpha_R = \alpha_T \Delta T \tag{10}$$

According to Eq.6, A_0 and B_0 are both proportional to ΔT (note that this is only approximately true because some other terms are also weak functions of temperature) and hence are proportional to α_R.

Table 2 shows experimental A_0 and B_0 for different channel heights both in nitrogen and helium flow while the overheat ratio remains 10%. To simplify the comparison, we used the same averaged n as in Table 1. From Eq.6 we have $A_0 \propto h^{-2/n}$. In Table 2 we only see that A_0 increases as h decreases. However it is difficult to tell how it changes with h from our data. One possible explanation is the change of h will affect the heat transfer in the channel and accordingly cause other parameters to change.

Table 2 Experimental A_0 and B_0 for different channel heights (a_R = 10% and n = 2.20)

gas	channel height	A_0	B_0
Nitrogen	150 μm	0.789	5.61
	200 μm	0.719	5.20
	288 μm	0.562	5.48
Helium	150 μm	1.51	7.25
	200 μm	1.31	6.87
	288 μm	0.847	7.38

Different gas properties will also affect the sensor sensitivity. It can be shown that $A_0 \propto k_T \alpha^{-1/n}$, where $\alpha = k_T / \rho c_p$ is the thermal diffusivity of the gas. For nitrogen, k_T = 2.59 × 10^{-2} W/m·K, α = 2.21 × 10^{-5} m^2/s and for helium, k_T = 0.152 W/m·K, α = 1.80 × 10^{-4} m^2/s. Let n be 2.20, we obtain the theoretical ratio of A_0 (He) over A_0 (N_2) is 2.26. From Table 1 and Table 2, we can see that all the experimental ratios are less than the theoretical value, which also implies that more parameter changes should be considered.

CONCLUSION

A novel two-mode mass flowmeter, which combines both thermal and differential pressure principles, has been successfully fabricated. This flowmeter is based on a multi-sensor chip that includes a 1-D array of shear stress, pressure and temperature sensors. By combining two complementary principles, the performance of the flowmeter can be significantly improved. The sensitivity of the thermal flowmeter is further improved by vacuum-cavity based thermal isolation. We also obtain the pressure, temperature and shear stress distributions in both incompressible and compressible channel flows. The multi-sensor chip is highly suitable in the study of some complex channel flows such as flow in micro nozzle. We also find the $P \propto t^{1/3}$ law for conventional hot film sensors is not valid for our micromachined shear stress sensor, and further study is needed. Extensive tests have been carried out on the

shear stress sensor with various overheat ratios, channel heights and gases.

ACKNOWLEDGEMENTS

This work is supported by JPL under account code 49-204-52000-0-3460. The authors would like to thank Shuyun Wu, Trevor Roper and Hung Bui for their help with the process, Xing Yang and Ellis Meng for helpful discussions.

REFERENCES

[1] A. F. P Van Putten, S. Middelhoek, "Integrated silicon anemometer", *Electronics Letters*, Vol. 10, No. 21, Oct 17 1974, pp. 425-426

[2] B. W. van Oudheusden, "Silicon thermal flow sensors", *Sensors and Actuators, A: Physical*, Vol. 30, No. 1-2 ,Jan 1992, pp. 5-26

[3] N. T. Nguyen, "Micormachined flow sensors – a review", *Flow Meas. Instrum.*, Vol. 8, No. 1, pp. 7-16, 1997

[4] C. Liu, Y. C. Tai, J. B. Huang, and C. M. Ho, "Surface Micromachined Thermal Shear Stress Sensor", *ASME International Mechanical Engineering Congress and Exposition*, Chicago, IL, pp. 9-15, Nov. 6-11 (1994).

[5] F. Jiang, Y. C. Tai, B. Gupta, R. Goodman, S. Tung, and C. H. Ho, "A Micromachined Shear Stress Imager", *MEMS96*, San Diego, pp. 110-115, 1996.

[6] F. Jiang, Y. C. Tai, K. Walsh, T. Tsao, G. B. Lee, and C. M. Ho, "A Flexible MEMS Technology and Its First Application to Shear Stress Sensor Skin", *MEMS97*, Nagoya Castle, Japan, pp. 465-470, 1997.

[7] J. Q. Liu, *Integrated Micro Devices for Small Scale Gaseous Flow Study*, Ph.D. Thesis, California Institute of Technology, 1995.

[8] R. J. Goldstein, *Fluid Mechanics Measurements*, 2nd Edition, Taylor & Francis, 1996

[9] F. M. White, *Fluid mechanics*, 2nd Edition, McGraw-Hill, 1986.

[10] Q. Lin, F. Jiang, X.Q. Wang, Z. Han, Y.C. Tai, J. Lew and C.M. Ho, "MEMS Thermal Shear-Stress Sensors: Experiments, Theory and Modeling", *2000 Solid-State Sensor and Actuator Workshop (Hilton Head 2000)*